Characterization and Dehydrogenation Activity of SBA-15 and HMS Supported Chromia Catalysts†

YUE, Hong-Yong(乐洪咏) ZHENG, Bo(郑波) YUE, Ying-Hong(乐英红)
ZHANG, Xue-Zheng(张雪峥) HUA, Wei-Ming(华伟明) GAO, Zi*(高滋)
Laboratory of Molecular Catalysis and Innovative Materials, Department of Chemistry, Fudan University, Shanghai 200433, China

SBA-15 and HMS supported chromia catalysts were prepared and characterized. Chromia is highly dispersed on the mesoporous supports when its loading is ≤7 wt%. The supported catalysts display high activity, selectivity and stability for dehydrogenation of ethylbenzene and propane. ESR measurement of the catalysts before and after reaction shows that the active species for dehydrogenation reaction might be Cr^{3+} species on the catalyst surface, and the activity of the catalyst is probably correlated with the dispersion of Cr^{3+} species.

Keywords SBA-15, HMS, supported chromia catalyst, ethylbenzene dehydrogenation, propane dehydrogenation

Introduction

Enormous study has been devoted to M41S, the first family of mesoporous molecular sieves reported in 1992,[1,2] including their modifications and applications in catalysis. The attractive properties of these materials are their high specific surface area (> 1000 m^2/g), well-defined structure and uniform pore size which can be tuned in the range of 1.5—10 nm. One obvious drawback restraining their use as catalysts or catalyst supports is their low hydrothermal stability[3-5] due to the thin amorphous oxide channel wall, which is only 0.8—0.9 nm in the case of MCM-41.[3,6] The mesostructure of MCM-41 even collapses in wet air at ambient temperature within three short months.[7] Adding salt to the reaction mixture during hydrothermal crystallization can improve the hydrothermal stability of MCM-41, yet the role of the salt in crystallization is not clear.[8]

HMS is another type of mesoporous molecular sieve prepared via a neutral templating route using primary amines as the templates.[9,10] The mesoporous structure of HMS is less ordered, but its wall thickness and textural mesoporosity are slightly higher than those of MCM-41. SBA-15 is a newly discovered mesoporous molecular sieve which synthesized by using a nonionic triblock co-polymer surfactant as the template.[11,12] The pore size of SBA-15 is in the range of 4.7—30 nm, and its wall thickness in the range of 3.1—6.4 nm. SBA-15 is more hydrothermally stable than MCM-41 and HMS due to its extremely thick channel wall. Aluminum has been incorporated into HMS and SBA-15 by direct synthesis[13,14] or post synthesis methods.[15,16] It is speculated that these two mesoporous molecular sieves, in particular SBA-15, might be better catalysts or catalyst supports than MCM-41.

In this work, SBA-15, and HMS supported chromia mesoporous molecular sieves were prepared. The dispersion of the metal oxide on the supports was studied by XRD and N_2 adsorption method. The dehydrogenation activities of the catalysts were tested using ethylbenzene and propane dehydrogenation as model reactions. The active species on the catalysts for dehydrogenation reaction was discussed with respect to ESR measurements of the cata-

* E-mail: zigao@fudan.edu.cn
Received April 1, 2002; revised July 10; accepted August 8, 2002.
Project supported by the Major State Basic Research Development Program of China (No. G2000077500) and the Foundation for University Key Teachers by the Education Ministry of China.
† Dedicated to Professor HUANG Yao-Zeng on the occasion of his 90th birthday.

lysts before and after reaction.

Experimental

Sample preparation

SBA-15 was prepared following the procedure reported by Zhao *et al*.[11] The template, $EO_{20}PO_{70}EO_{20}$ (Aldrich) (4.0 g), was dissolved in distilled water (30.0 g), and then HCl aqueous solution (120 g, 2 mol/L) was added. After the template solution was heated to 40 ℃, tetraethylorthosilicate (TEOS) (8.5 g) was added dropwise with stirring. The mixture (pH < 2) was stirred for another 3 h and allowed to react statically at 100 ℃ for 48 h. The product was filtered, washed with distilled water, and dried at ambient temperature. To remove the organic template, calcination was carried out first at 150 ℃ for 1 h, and then the temperature was slowly increased to 500 ℃ and kept at 500 ℃ for 6 h.

HMS was synthesized according to the method described by Pinnavaia *et al*.[9] Mixture A was obtained by dissolving TEOS (10.4 g) in a co-solvent of EtOH (15.0 g) and *iso*-propanol (*i*-PrOH) (3.0 g). Mixture B was obtained by dissolving hexadecylamine (HDA) (3.3 g) in distilled water (32.4 g). Mixture B was added to mixture A under vigorous agitation which continued for another 1—2 h. The molar ratio of the starting materials was as follows: TEOS:HDA:*i*-PrOH:EtOH:H_2O = 1:0.27:1:6.5:36. The new mixture underwent static crystallization at ambient temperature for 72 h. After filtration, washing and desiccation, the resulting solid powder was calcined in air at 540 ℃ for 6 h to burn off the surfactant.

Chromia was impregnated onto SBA-15 and HMS via an incipient wetness method. Aqueous solutions with varied amount of chromium nitrate were applied to calcined SBA-15 or HMS, followed by drying and calcining at 500 ℃ for 5 h in air. The catalysts were designated as $Cr_2O_3(x)$/support, where x represented the weight percentage of Cr_2O_3 in the catalysts.

Characterization

The textural properties of all the samples, which were outgassed at 350 ℃ in advance, were measured on a Micromeritics ASAP 2000 equipment at liquid-nitrogen temperature using N_2 as the adsorbent. The pore size distributions were calculated with BJH method. X-Ray diffraction (XRD) patterns were collected on a Rigaku D/MAX-IIA instrument with Cu Kα radiation at 40 kV and 20 mA. Electron spin resonance (ESR) spectra of the samples were acquired on a Bruker ER200D-SRC instrument at 120 K in the X-band region scanning from 0—6000 Gauss with the magnetic field centered at 3000 Gauss.

Activity test

The dehydrogenation reactions were conducted in a fixed-bed flow microreactor at ambient pressure. For ethylbenzene dehydrogenation, the catalysts (100 mg) granulated into 40—60 mesh were activated in N_2 at 500 ℃ for 3 h before reaction. Ethylbenzene was fed into the reactor from a saturator at 0 ℃ by flowing N_2 with a rate of 10 mL/min, and the reaction temperature was 773 K. For propane dehydrogenation, the catalyst load was 200 mg, and it was pretreated at 823 K for 0.5 h in oxygen flow, and then at 623 K for 0.5 h in hydrogen flow. The reactant contained 2.5 mol% propane and balancing nitrogen, and the reaction was run at 823 K under a flow rate of 20 mL/min. The products were analyzed by an online gas chromatograph equipped with a flame ion detector (FID) and a 2 m-column of DNP for ethylbenzene dehydrogenation and a 6 m-column of Porapak Q for propane dehydrogenation.

Results and discussion

Catalyst characterization

XRD patterns of the synthesized mesoporous supports and the supported catalysts at low angle region are shown in Figs. 1 and 2. SBA-15 gives five well-resolved peaks that can be indexed as (100), (110), (200), (210) and (300) diffraction peaks associated with *p6mm* hexagonal symmetry. In contrast, only one (100) diffraction peak is observed in the XRD pattern of HMS, and higher order Bragg reflections of the hexagonal structure are not resolved, demonstrating that the structure of HMS is more disordered as compared with that of SBA-15. As the chromia loading is increased, the intensity of the characteristic reflection peaks of SBA-15 and HMS is reduced, and the peaks vanish at chromia loading of 20 wt%. The decrease in intensity is probably caused by the large X-ray mass absorption coefficient of chromium (260

cm^2/g) in comparison to that of silicon (60.6 cm^2/g) and oxygen (11.5 cm^2/g).[17]

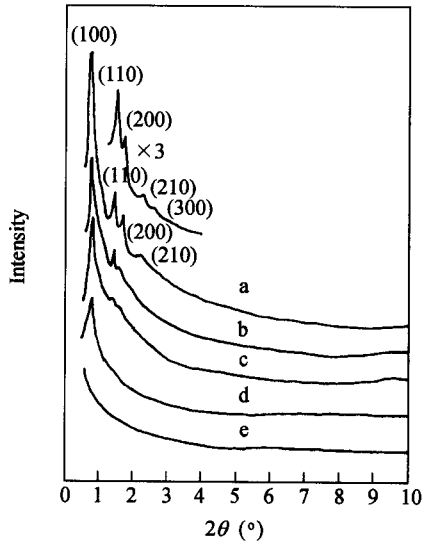

Fig. 1 Low-angle XRD patterns of (a) SBA-15, (b) Cr_2O_3(3)/SBA-15, (c) Cr_2O_3(7)/SBA-15, (d) Cr_2O_3(11)/SBA-15, (e) Cr_2O_3(20)/SBA-15.

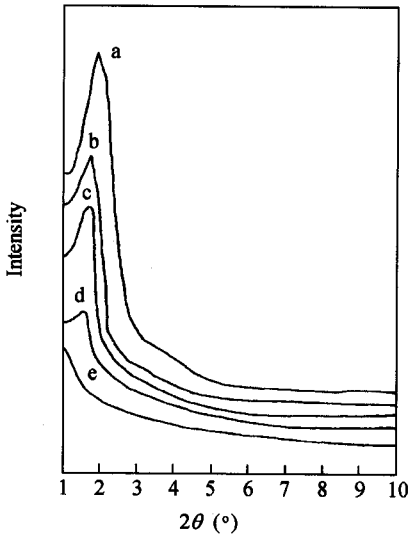

Fig. 2 Low-angle XRD patterns of (a) HMS, (b) Cr_2O_3(3)/HMS, (c) Cr_2O_3(7)/HMS, (d) Cr_2O_3(11)/HMS and (e) Cr_2O_3(20)/HMS.

The wide angle X-ray diffraction patterns of the samples were recorded as well. The two series of samples display similar results, so only the patterns of Cr_2O_3/SBA-15 catalysts are given in Fig. 3. X-Ray reflections of Cr_2O_3 crystallites are observed when the chromia content in the sample is above 7 wt%, showing that chromia is highly dispersed on the mesoporous supports when its loading is below 7 wt%. Similar result was observed on chromia supported MCM-41 catalysts.[18]

The N_2 adsorption/desorption isotherms of the samples are depicted in Figs. 4 and 5. All isotherms are of type IV with a typical H1 hysteresis loop. The hysteresis loop of the SBA-15 series catalysts appears in

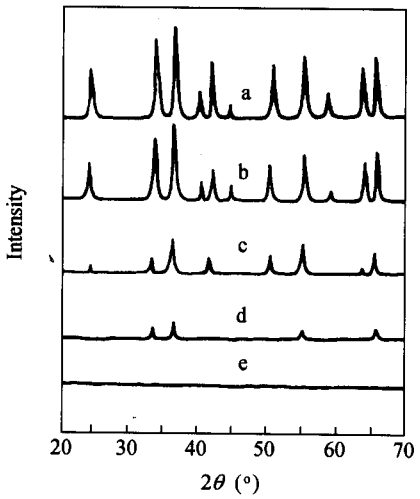

Fig. 3 Wide-angle XRD patterns of (a) Cr_2O_3, (b) Cr_2O_3(20)/SBA-15, (c) Cr_2O_3(11)/SBA-15, (d) Cr_2O_3(9)/SBA-15, (e) Cr_2O_3(7)/SBA-15.

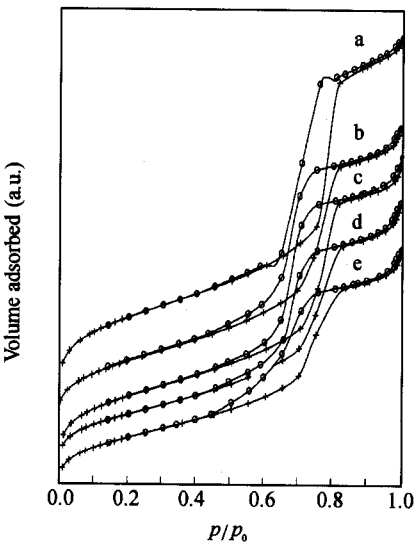

Fig. 4 Nitrogen adsorption/desorption isotherms of (a) SBA-15, (b) Cr_2O_3(3)/SBA-15, (c) Cr_2O_3(7)/SBA-15, (d) Cr_2O_3(11)/SBA-15 and (e) Cr_2O_3(20)/SBA-15.

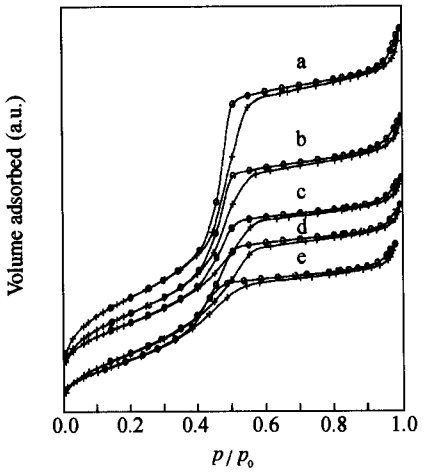

Fig. 5 Nitrogen adsorption/desorption isotherms of (a) HMS, (b) Cr_2O_3 (3)/HMS, (c) Cr_2O_3 (7)/HMS, (d) Cr_2O_3(11)/HMS and (e) Cr_2O_3(20)/HMS.

the p/p_0 range of 0.5—0.8 whereas that of the HMS series catalysts in the p/p_0 range of 0.4—0.6, indicating that the pore sizes of the SBA-15 series are larger than those of the HMS series. The textural properties of the samples derived from the isotherms are listed in Table 1. The specific surface area, pore volume and pore diameter of the chromia supported catalysts decrease with the increase of chromia content, but the textural parameters of the Cr_2O_3/SBA-15 series decrease much slower than those of the Cr_2O_3/HMS series, implying that the larger channels in SBA-15 help to prevent the porous support from obstruction with incorporated chromia crystallites.

Dehydrogenation of ethylbenzene

Dehydrogenation of ethylbenzene is an important process in petrochemical industry. Under our reaction conditions, the dehydrogenation reaction achieves steady state after 7 h on stream over the catalysts, and the selectivity of the catalysts to styrene is always above 97%. The steady state reaction data of the two series of catalysts are listed in Table 2 and compared with those of bulk Cr_2O_3 and CrO_3. The supported chromia catalysts are much more active than the bulk oxides. The ethylbenzene conversion of the catalysts increases with chromia loading at first and then remains at a plateau. The ethylbenzene conversion of the Cr_2O_3/SBA-15 series is slightly higher than that of the Cr_2O_3/HMS series with the same chromia loading due to the larger pore size of SBA-15, which facilitates the internal diffusion of the reactant and the products during reaction.

The stability of Cr_2O_3(7)/SBA-15, Cr_2O_3(7)/HMS and Cr_2O_3(7)/Al_2O_3 catalysts in ethylbenzene dehydrogenation reaction was studied and the results are listed in Table 3. The steady state activity of the catalysts is Cr_2O_3 (7)/SBA-15 $\approx$ Cr_2O_3(7)/γ-Al_2O_3 > Cr_2O_3(7)/HMS. However, after reaction for 60 h, the activity order changes to Cr_2O_3(7)/SBA-15 > Cr_2O_3(7)/γ-Al_2O_3 > Cr_2O_3(7)/HMS, showing that Cr_2O_3(7)/SBA-15 is probably more resistant to coking and sintering due to the large pore size and high surface area of the support.

Table 1 Textural properties of chromia supported catalysts

Catalyst	BET surface area (m^2/g)	Pore volume (cm^3/g)	Pore diameter (nm)
SBA-15	760	1.17	6.5
Cr_2O_3(1)/SBA-15	643	0.86	6.5
Cr_2O_3(3)/SBA-15	644	0.96	6.5
Cr_2O_3(7)/SBA-15	624	0.91	6.4
Cr_2O_3(11)/SBA-15	529	0.82	6.3
Cr_2O_3(20)/SBA-15	528	0.76	6.3
HMS	952	1.10	4.0
Cr_2O_3(1)/HMS	846	1.09	3.8
Cr_2O_3(3)/HMS	739	0.85	3.8
Cr_2O_3(7)/HMS	620	0.65	3.8
Cr_2O_3(11)/HMS	597	0.65	3.5
Cr_2O_3(20)/HMS	487	0.52	3.2

Dehydrogenation of propane

Dehydrogenation of propane is another commercially interesting catalytic reaction. Chromia supported on various oxides, such as γ-Al_2O_3, SiO_2 and ZrO_2, are well-known active catalysts.[19-21] The activity of SBA-15 and HMS supported chromia catalysts for this reaction was investigated. Their steady state activity and selectivity achieved after reaction for 6 h on stream are listed in Table 4, together with the data of bulk chromium oxides and Cr_2O_3/γ-Al_2O_3 catalysts for comparison. Similar to the situation in dehydrogenation of ethylbenzene, the supported catalysts are much more active than bulk Cr_2O_3 and CrO_3. The catalytic activity of supported catalysts with the same Cr_2O_3 loading follows the order of Cr_2O_3/SBA-15 $\approx$ Cr_2O_3/HMS > Cr_2O_3/γ-Al_2O_3.

The stability of different supported catalysts in this reaction was also studied and the results are shown in Fig. 6. Even though the initial activity of $Cr_2O_3(7)$/HMS is higher than that of $Cr_2O_3(7)$/SBA-15, it deactivates faster during reaction. After reaction for 60 h, the activity order of the catalysts is $Cr_2O_3(7)$/SBA-15 > $Cr_2O_3(7)$/HMS > $Cr_2O_3(7)/\gamma$-Al_2O_3.

Table 2 Steady state activities of various catalysts for dehydrogenation of ethylbenzene

Catalyst	Conversion (%)	Activity [mmol/(h·$g_{Cr_2O_3}$)]	Selectivity (%)
$Cr_2O_3(1)$/SBA-15	36.0	23.2	99.7
$Cr_2O_3(3)$/SBA-15	81.2	17.4	98.2
$Cr_2O_3(7)$/SBA-15	87.5	8.04	97.3
$Cr_2O_3(11)$/SBA-15	84.7	4.95	97.4
$Cr_2O_3(20)$/SBA-15	85.6	2.75	97.7
$Cr_2O_3(1)$/HMS	38.8	25.0	98.9
$Cr_2O_3(3)$/HMS	67.9	14.6	99.0
$Cr_2O_3(7)$/HMS	82.3	7.56	97.5
$Cr_2O_3(11)$/HMS	80.6	4.71	98.1
$Cr_2O_3(20)$/HMS	81.2	2.61	98.4
Cr_2O_3	13.5	0.09	100
CrO_3	25.0	0.25	98.6

Table 3 Stability of chromia supported catalysts in ethylbenzene dehydrogenation

Catalyst	Conversion (%)		Activity [mmol/(h·g)]		Selectivity (%)	
	initial	60 h	initial	60 h	initial	60 h
$Cr_2O_3(7)$/SBA-15	87.5	78.8	8.04	7.22	97.3	98.8
$Cr_2O_3(7)$/HMS	82.3	67.8	7.56	6.22	97.5	99.1
$Cr_2O_3(7)/\gamma$-Al_2O_3	87.2	74.8	7.62	6.87	99.4	100

Table 4 Steady state activities of various catalysts for dehydrogenation of propane

Catalyst	Conversion (%)	Activity [mmol/(h·$g_{Cr_2O_3}$)]	Selectivity (%)
$Cr_2O_3(3)$/SBA-15	19.9	40.7	92.8
$Cr_2O_3(7)$/SBA-15	24.5	21.5	96.3
$Cr_2O_3(3)$/HMS	18.4	37.6	94.6
$Cr_2O_3(7)$/HMS	25.0	22.0	96.0
$Cr_2O_3(3)/\gamma$-Al_2O_3	10.2	20.9	93.2
$Cr_2O_3(7)/\gamma$-Al_2O_3	22.6	19.8	96.5
Cr_2O_3	5.4	0.33	91.9
CrO_3	7.1	0.66	87.7

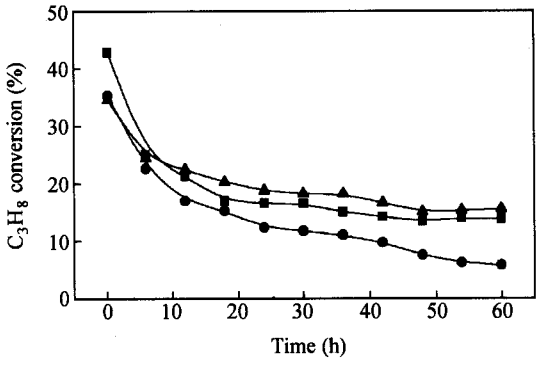

Fig. 6 Propane conversion on supported chromia catalysts as a function of time on stream. (▲) $Cr_2O_3(7)$/SBA-15, (■) $Cr_2O_3(7)$/HMS, (●) $Cr_2O_3(7)/\gamma$-Al_2O_3.

ESR *studies*

The surface composition of supported chromia catalysts is rather complicated. Cr^{6+}, Cr^{5+}, Cr^{3+} and Cr^{2+} species have been detected on these catalysts by XPS, DRS (diffuse reflectance spectroscopy) and ESR methods.[21] Their relative concentrations depend on the overall Cr loading, the nature of the support and the pretreatment conditions. Owing to the complexity of the problem the nature of the active species for various dehydrogenation reactions remains a matter of controversy.

$Cr_2O_3(7)$/SBA-15 and $Cr_2O_3(7)$/HMS were subjected to ESR measurement before and after reaction. The ESR spectra of the two catalysts are similar, so only the spectra of $Cr_2O_3(7)$/SBA-15 are shown in Fig. 7. In previous work,[22,23] γ ($g = 1.97$), β ($g = 1.96$—2.45) and δ ($g = 3.5$—5.5) signals were observed on the spectra of supported chromia catalysts, and the γ, β and δ signals were assigned to mononuclear Cr^{5+}, clustered Cr^{3+} and isolated Cr^{3+}, respectively. Before reaction, a sharp symmetric γ signal with $g = 1.974$ and a weak δ signal with $g = 4.31$ are observed on the spectrum of $Cr_2O_3(7)$/SBA-15. The presence of β signal is uncertain, because it might be covered by the strong γ signal. After 7 h of ethylbenzene dehydrogenation reaction, the γ signal reduces considerably, and a broad β signal with $g = 2.25$ and three small signals with g values of 1.97, 1.983 and 2.003 appear in the vicinity of the original γ signal. According to Groeneveld *et al.*,[24] the γ_1 ($g = 1.978$), γ_2 ($g = 1.983$) and γ_1 ($g = 2.003$) signals can be attributed to square-pyramidally coordinated Cr^{5+}, distorted tetrahedrally coordinated Cr^{5+} and Cr^{3+} in Cr_2O_3 crystallites, respectively. After 60 h of the reaction, the intensities of γ_1 and γ_2 signals further reduce, whereas that of γ_1 signal is slightly increased. Correlating the change in ESR spectra with that in activity during reaction, it can be suggested that the dehydrogenation active species are surface Cr^{3+} oxide species. The initially formed high valency species Cr^{6+} and Cr^{5+} on the catalyst do not remain for a long time on stream. Most of them are reduced to Cr^{3+} species in the reaction environment before steady state is reached. On the other hand, the decrease in dehydrogenation activity during reaction might be related with chromia dispersion as well as coking on the catalysts, *i.e.*, the isolate Cr^{3+} species and the clustered Cr^{3+} species are probably more active than the Cr^{3+} species in Cr_2O_3 crystallites. Hence, the activity of the supported chromia catalysts decreases as the β_1 signal is increased. This suggestion is consistent with the observation of many authors.[25]

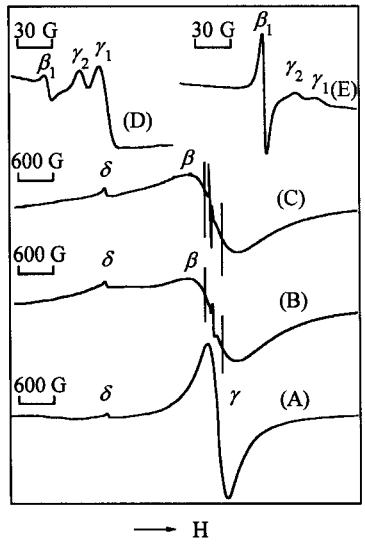

Fig. 7 ESR spectra of $Cr_2O_3(7)$/SBA-15. (A) before reaction, (B) after 7 h of reaction, (C) after 60 h of reaction, (D) the magnified profile of the marked segment in B, (E) the magnified profile of the marked segment in C.

Conclusions

SBA-15 and HMS mesoporous molecular sieves are good supports for dehydrogenation catalysts due to their high surface area and large mesoporosity. Metal oxides such as Cr_2O_3 can be highly dispersed on these supports

with a loading as high as 7 wt%. The supported chromia catalysts display high activity, selectivity and stability for ethylbenzene and propane dehydrogenation. The performance of Cr_2O_3/SBA-15 in long term reactions is superior to the other supported catalysts including the widely used industrial Cr_2O_3/γ-Al_2O_3 catalyst.

References

1 Kresge, C. T.; Leonowicz, M. E.; Roth, W. J.; Vartuli, J. C.; Beck, J. S. *Nature* **1992**, *359*, 710.

2 Beck, J. S.; Vartuli, J. C.; Roth, W. J.; Leonowicz, M. E.; Kresge, C. T.; Schmitt, K. D.; Chu, C. T-W.; Olson, D. H.; Sheppard, E. W.; McCullen, S. B.; Higgins, J. B.; Schlenker, J. L. *J. Am. Chem. Soc.* **1992**, *114*, 10834.

3 Chen, C. Y.; Li, H. X.; Davis, H. E. *Microporous Mater.* **1993**, *2*, 17.

4 Kim, J. M.; Kwak, J. H.; Jim, S.; Ryoo, R. *J. Phys. Chem.* **1995**, *99*, 16742.

5 Ryoo, R.; Kim, J. M.; Ko, C. H.; Shin, C. H. *J. Phys. Chem.* **1996**, *100* , 17718.

6 Monnier, A.; Schuth, F.; Huo, Q.; Kumar, D.; Margolese, D.; Maxell, R. S.; Stucky, G. D.; Krishnamurty, M.; Petroff, P.; Firouzi, A.; Janicke, M.; Chmelka, B. F. *Science* **1993**, *261*, 1299.

7 Li, H. Y.; Sun, Y.; Yue, Y. H.; Gao, Z. *Chem. J. Chin. Univ.* **1999**, *20*, 272 (in Chinese).

8 Ryoo, R.; Jun, S. *J. Phys. Chem. B* **1997**, *101*, 317.

9 Tanev, P. T.; Chibwe, M.; Pinnavaia, T. J. *Nature* **1994**, *368*, 321.

10 Tanev, P. T.; Pinnavaia, T. J. *Science* **1995**, *267*, 865.

11 Zhao, D.; Feng, J.; Huo, Q.; Melosh, N.; Fredrickson, G. H.; Chmelka, B. F.; Stucky, G. D. *Science* **1998**, *279*, 548.

12 Zhao, D.; Huo, Q.; Feng, J.; Chmelka, B. F.; Stucky, G. D. *J. Am. Chem. Soc.* **1998**, *120*, 6024.

13 Yue, Y.; Sun, Y.; Xu, Q.; Gao, Z. *Appl. Catal. A.* **1998**, *175*, 131.

14 Yue, Y.; Gedeon, A.; Bonardet, J.; Melosh, N.; D'Espinose, J.; Fraissard, J. *Chem. Commun.* **1999**, 1967.

15 Luan, Z.; Hartmann, M.; Zhao, D.; Zhou, W.; Kevan, L. *Chem. Mater.* **1999**, *11*, 1621.

16 Cheng, M.; Wang, Z.; Sakurai, K.; Kumata, F.; Saito, T.; Komatsu, T.; Yashima, T. *Chem. Lett.* **1999**, *2*, 131.

17 Klug, H. P.; Alexander, L. E. In *X-Ray Diffraction Procedures for Polycrystalline and Amorphous Materials*, John Wiley & Sons, New York, **1974**.

18 He, J.; Duan, X.; Howe, R. F. *Acta Chim. Sinica* **1999**, *57*, 125 (in Chinese).

19 De Rossi, S.; Ferraris, G.; Fremiotti, S.; Cimino, A.; Indovina V. *Appl. Catal. A* **1992**, *81*, 113.

20 De Rossi, S.; Ferraris, G.; Fremiotti, S.; Cimino, A.; Garrone, E.; Ghiotti, G.; Campa, M. C.; Indovina, V. *J. Catal.* **1994**, *148*, 36.

21 Weckhuysen, B. M; Schoonheydt, R. A. *Catal. Today* **1999**, *51*, 223.

22 Weckhuysen, B. M; Schoonheydt, R. A.; Mabbs, F. E.; Collison, D. *J. Chem. Soc., Faraday Trans.* **1996**, *92*, 2431.

23 Weckhuysen, B. M.; Ridder, L. M.; Grobet, P. T.; Schoonheydt, R. A. *J. Phys. Chem.* **1995**, *99*, 320.

24 Groeneveld, C.; Wittgen, P. P. M. M.; Kersbergen, A. M.; Mestrom, P. L. M.; Nuijten, C. E. *J. Catal.* **1979**, *59*, 153.

25 Mentasty, L. R.; Gorriz, O. F.; Cadus, L. E. *Ind. Eng. Chem. Res.* **1999**, *38*, 396.

(E0204014 SONG, J. P.; HUANG, W. Q.)